Spin-coated fluorinated PbS QD superlattice thin film with high hole mobility

SCHOLARONE™
Manuscripts

Spin-coated fluorinated PbS QD superlattice thin film with high hole mobility

Pan Xia,[1] Daniel W. Davies,[2] Bijal B. Patel,[2] Maotong Qin,[3] Zhiming Liang,[4] Kenneth R. Graham,[4] Ying Diao,[2] and Ming Lee Tang[1,]*

[1] Department of Chemistry & Materials Science and Engineering Program, University of California, Riverside, 900 University Avenue, Riverside, California 92521, United States
[2] Department of Chemical and Biomolecular Engineering, University of Illinois at Urbana−Champaign, 600 South Mathews Avenue, Urbana, Illinois 61801, United States
[3] Department of Materials Chemistry, School of Chemistry and Materials Science, University of Science and Technology of China, NO. 96 Jinzhai Road, Hefei, Anhui, 230026 P. R. China
[4] Department of Chemistry, University of Kentucky, Lexington, Kentucky 40506, United States

Abstract

Motivated by the oleophobic and electron-withdrawing nature of perfluorocarbons, we explore the effect of a trifluoromethyl coating on lead sulfide quantum dots (PbS QDs) in thin film transistor (TFT) geometry. The low surface energy conferred by the oleophobic perfluorocarbons creates QDs packed in a primitive cubic lattice with long range order, as confirmed by grazing incidence small angle x-ray scattering (GISAXS) and transmission electron microscopy (TEM). Hole mobilities as high as 0.085 cm^2/ Vs were measured in the TFTs. No electron transport was observed. This suggests that the electron-withdrawing nature of the trifluoromethyl ligand is eclipsed by the excess holes present in the PbS QDs that likely stem from cation vacancies induced by the thiol group.

Key words

superlattice, quantum dots, film transistor, fluorine, lead sulfide

The large surface area intrinsic to semiconductor quantum dots (QDs), where approximately one-third of the atoms/ ions are on its exterior, makes the prospect of tuning the ligand shell to modify its physical and electronic properties appealing. Ideally, short ligands that can promote electronic coupling between particles in thin film would be used to engineer the surface energetics and electronic energy levels of QDs to induce mesoscale order. Furthermore, in terms of ligand selection, these short ligands should not compromise the colloidal stability of QD inks to allow solution processed thin films to be fabricated easily.

Various ligand treatments on QD thin films have been conducted to promote electronic coupling and passivate trap states.[1-6] Treatments include elemental indium[7, 8], organic halides[9-12], metal halides[13-15] and pseudohalides[16-18]. Benzenedithiol or other aliphatic thiols like mercaptopropionic acid (MPA) are routinely used to cross-link QD thin films because of their natural affinity with the QD chalcogenide lattice[14, 19-22]. Short-chain thiols are necessary because QDs are synthesized with long-chain, aliphatic chains that confer colloidal stability at the expense of conductivity. Thiol treatment results in a thin film that allows charge to percolate, typically via a hopping mechanism. A variable range hopping model was used by Law et al to explain the lack of correlation between transistor mobility and sample polydispersity. Law et al postulate that holes or electrons hop through states on the largest QDs in the thin film[23]. Others have used halides or pseudohalides[12, 16, 24] to draw the QDs closer together. For example, in 2012, the Sargent group used CdCl$_2$ to minimize mid-gap states for record QD solar cell power conversion efficiencies (PCEs) of 7%[14]; in 2016, methyl ammonium iodide for 10.6% certified PCE[10]; in 2018, a PbI$_2$ matrix improved the

the PCE to 12%[25]. Despite these improvements, observations of band transport in QD thin films remain controversial. For example, two reports of QD TFTs, one from the Kagan group using thiocyanate[26], and one from the Talapin group using $In_2Se_4^{2-}$ ligands[27], show increasing mobility with decreasing temperature, observations associated with band transport[28]. However, the high mobilities measured can be shown in the context of Marcus theory to be due to phonon-assisted hoping because the calculated electronic coupling energy was much smaller than the reorganization energy[29]. Thus, it remains challenging to find a short ligand for QDs that can electronically passivate surface defects while promoting efficient charge transport.

Notwithstanding the fact that the QD-organic interface is complicated by dangling bonds, unpassivated surface sites, curvature induced strain, etc., we chose perfluorocarbons as the short ligands. We chose to use the trifluoromethyl containing group, CF_3-, for device applications, not only because it is a short ligand, but also due to the electronegativity of fluorine and previous reports that perfluoro ligands increase the air stability of nanocrystal thin films [30]. The compact fluorinated ligands are expected to facilitate wavefunction overlap between the QDs for efficient energy and charge transfer by replacing the original long insulating ligands. In addition, the electron withdrawing CF_3 group may be able to tune the band edges of the QDs to introduce a depletion region to promote the drift of charge carriers under short circuit conditions in a solar cell. The resultant band alignment might minimize recombination of photo-generated electrons at the anode. Both these factors should increase the photocurrent of the QD solar cell. This was the basis of a 2013 report by the Bawendi group where a combination of iodide and ethanethiol were used to control the band alignment in a PbS QD solar cell[31].
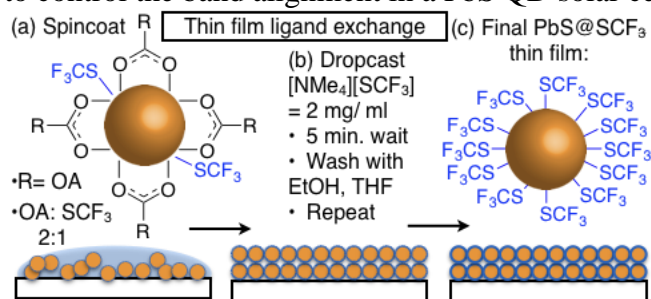

Figure 1. (a) Partially ligand exchanged PbS QDs were spin-coated on bottom contact transistor substrates. (b)Ligand exchange was performed on the resultant thin film to completely install the SCF_3 ligand and induce long range order Free ligands were removed with solvent to create (c) the resultant PbS–SCF_3 thin film. OA = oleic acid.

1) Preparation of superlattice thin film

Here, we report a spincoating method to fabricate electronically coupled PbS QD superlattice thin films with the trifluoromethanethiolate ligand ($\ominus SCF_3$) [32]. $\ominus SCF_3$ was chosen because it is a short ligand (<0.2 nm) that could potentially induce electronic wavefunction overlap in thin film. As shown in **Figure 1a**, partially ligand-exchanged colloidal PbS QDs with a ratio of native oleic acid (OA) to $\ominus SCF_3$ ligands of 2:1 were spin coated in a nitrogen atmosphere on bottom contact patterned substrates coated with self-assembled monolayers (SAMs) 3-mercaptopropyl trimethoxysilane (3-MPTMS) or 1H,1H,2H,2H-perfluorodecyltriethoxysilane. The absorption and photoluminescence (PL) of the partially ligand exchanged PbS QDs are shown in Fig. S1. Two consecutive ligand exchanges on this spin-coated thin film were performed by soaking the existing thin film in an acetonitrile solution of the [NMe_4][SCF_3] salt. Excess ligand was removed by spin-coating, followed by three washing steps: twice with ethanol and finally with tetrahydrofuran (Fig.

1b). This is Method 3 in Table S0 in the supporting information. ATR-IR measurements of PbS–SCF$_3$ verify the complete removal of OA after two cycles of ligand exchange in thin film.[32]
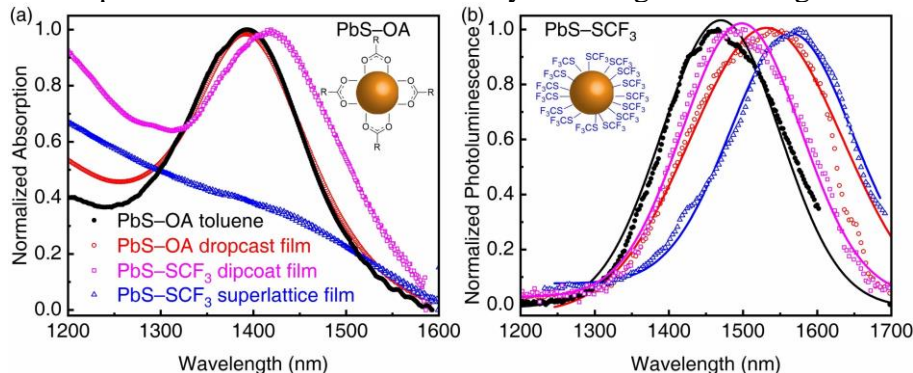

Figure 2. The absorption and photoluminescence (PL) of the PbS QDs. The original oleic acid (OA) capped PbS QDs in toluene (black filled circles) were-dropcast to make two thin films. One with OA ligands only (red open circle) and the other soaked in [NMe$_4$][SCF$_3$] solution (magenta squares) to compare with thin films made by spin-coating in **Figure 1** (blue triangle). The solid line in Figure 1b is a Gaussian fit of the QD PL.

2) Optical characterization of thin film

The PbS–SCF$_3$ thin film fabricated as illustrated in Figure 1 has a narrower photoluminescence (PL) peak compared to a dropcast thin film of the original OA capped PbS QDs. Table S0 summarizes the difference in PbS–SCF$_3$ thin film fabrication procedures. When PbS–OA QDs in toluene (filled black circles, Fig. 2), are dropcast to make a thin film (open red circles, Fig. 2, Method 0 Table S0), no change in the absorption maxima was observed since the dielectric environment created by oleic acid is similar to toluene. However, a red shift of 60 nm in the PL of the thin film compared to toluene was observed. This was previously observed by Kagan et al and explained as Forster energy transfer from small QDs to larger QDs within the ensemble.[33] The PbS–SCF$_3$ thin film made by the thin-film ligand exchange in Fig. 1 is termed the 'superlattice film' (blue triangles, Fig. 2, Method 3 Table S0). No absorption maxima was observed in this PbS–SCF$_3$ thin film, perhaps due to the low optical density of the 40 nm thin film. Alternatively, Loi et al propose that a decreased oscillator strength in PbS QD thin films stem from an altered dielectric environment or a broadening due to inhomogeneous electronic coupling.[34] To compare the effect of different ligand exchange procedures, we soaked the dropcast PbS–OA QD thin film in [NMe$_4$][SCF$_3$] in acetonitrile solution to completely replace OA with $\ominus$SCF$_3$ (Method 1 Table S0). This will be referred to as the 'PbS–SCF$_3$ dipcoat film', depicted for example in magenta squares in Fig. 2. The absorption maxima of this dipcoated PbS–SCF$_3$ film (magenta squares, Fig. 2) is red-shifted by more than 20 nm compared to PbS–OA due to the extra layer of thiolate from $\ominus$SCF$_3$ on QD surface. However, compared to the PL of the dropcast PbS–OA film, the PL of this dipcoat PbS–SCF$_3$ film is blue shifted, while the PL is red-shifted for the PbS–SCF$_3$ superlattice thin film. Most noticeably, the full width of half maximum (FWHM) of both PbS–SCF$_3$ thin films are 160 $\pm$ 2nm, smaller than the 207$\pm$ 4nm FWHM of the PL of the dropcast PbS−OA. This decreased FWHM could be due to enhanced self-reabsorption when the QDs are closer to each other in thin film within their Forster distance. On the other hand, the narrower FWHM may be due to an improved homogeneity of QDs where the $\ominus$SCF$_3$ ligand narrows the size and shape distribution in the original PbS QDs. A similar argument has been put forth by the Sargent group when PbI$_2$ monolayers on PbS QDs were used to fabricate state-of-the-art QD solar cells.[25] In their

work, the PbI_2 matrix increases the carrier diffusion length by decreasing the spread in energy levels between QDs via increasing particle homogeneity.

3) Thin film characterization with TEM and GISAXS

In order to characterize the long-range order in the $PbS–SCF_3$ thin films, GISAXS was performed. To determine the unit cell parameters, diffraction patterns were simulated using GIXSGUI[35] and were fit iteratively to achieve agreement between simulated and experimental peaks[36]. The experimentally obtained diffraction pattern overlaid with simulated is shown in Figure S2, S3 and S4. Through this procedure, we determined a cubic lattice with a lattice constant of 5.8 nm. We note that the specific space group and symmetry cannot be determined due to the limited number of peaks. The peak indexing results are shown in **Figure 3**, from which we can infer there are two orientations of the cubic lattice. We first discuss the $PbS–SCF_3$ superlattice thin films (Fig. 2, blue triangles) made as shown in Fig. 1. In Fig. 3a the superlattice thin film is unannealed, while in Fig. 3b, it is annealed at 60ºC. For the unannealed thin film in Fig. 3a, the dominant orientation occurs with the (101) plane parallel to the substrate (indexed in white). A second orientation with the (111) plane parallel to the substrate is indexed in red and exhibits weaker intensity, indicating this orientation occurs less frequently within the sample. Seen in **Figure 3b**, annealed samples appear to have the same cubic structure, though the weaker peaks from the (111) orientation seem to have disappeared. At the same time, the peak widths were reduced. Both observations indicate increased out of plane alignment of the crystalline domains after annealing, which may contribute to enhanced charge transport. In comparison, the GISAXS pattern of the $PbS–SCF_3$ dipcoat sample (**Figure 3c**) exhibits a dominant (111) orientation instead of the (101) orientation seen from spincoating (**Figure 3b**). This becomes clear in Figure S3 that compares the fits for both orientations and shows close agreement with the (111) orientation. Further, we see from the normalized intensities in Figure S4 there appears to be a reduction in crystallinity from the nonannealed spincoated to the dipcoated samples. The (101) and (111) orientations are drawn in Fig. 3d and 3e respectively. From previous work, dipcoating can result in amorphous thin films due to an isotropic contraction when the long OA are replaced with the short $\ominus SCF_3$ ligands.[37-39] However, like reported by Gaulding et al[40], our dipcoated film also shows long range order, albeit with reduced crystallinity compared to the purely spin-coated thin film.
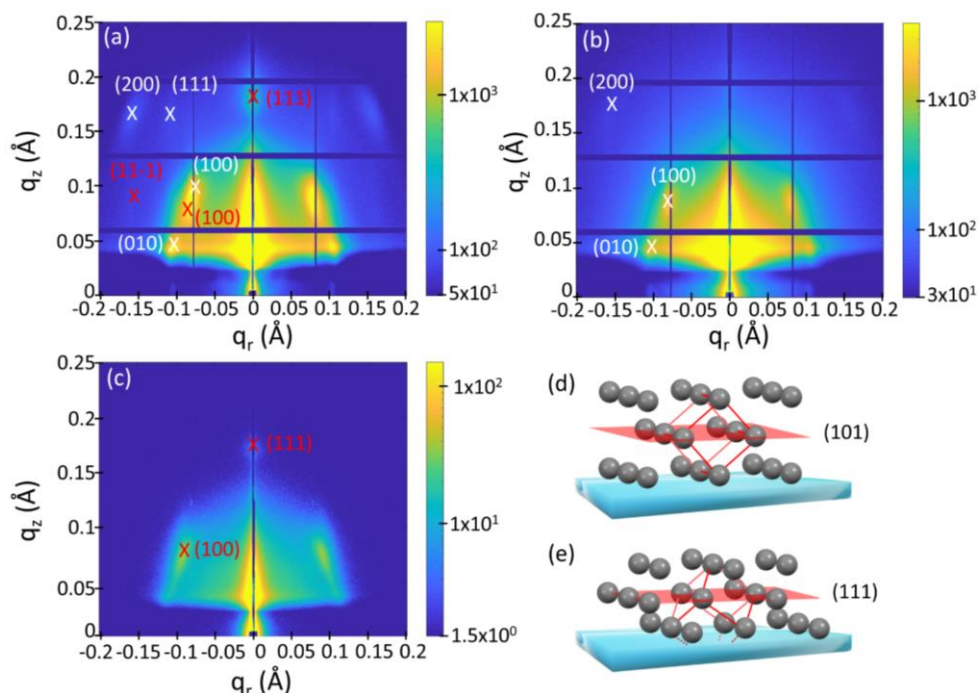
Figure 3. GISAXS for (a) nonannealed spincoated, (b) annealed spincoated and (c) nonannealed dipcoated PbS–SCF₃ thin films show a cubic lattice with a lattice constant = 5.8 nm. The diffraction peaks from the orientation with (101) parallel to the substrate are indexed in white and the peaks from the orientation with (111) parallel to the substrate are indexed in red. Note that for the (111) orientation, the (100) peak also appears at a similar position as the case of (101) orientation (Figure S2). All of the diffraction patterns shown were taken at X-ray incident angle of 0.2°. (d) and (e) show the (101) and (111) lattice orientations with respect to the substrate with the unit cell orientation indicated in red.
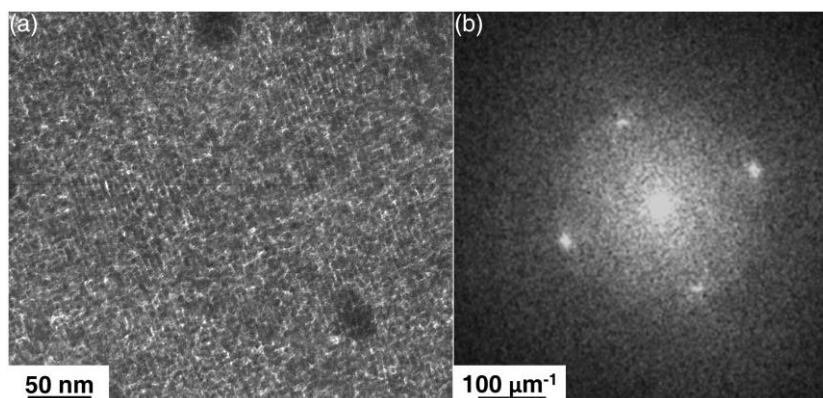

Figure 4. (a) Transmission electron micrographs show a PbS−SCF₃ superlattice made by spincoating without annealing, method 3 Table S0) with distance between two QDs of 5.6 ± 0.5 nm. The fast-Fourier transfer (FFT) of the real space image gives two pairs of peaks with ratio of the distances between the peaks ~1.5, close to the expected 1.41 for the (101) plane perpendicular to the substrate.

Transmission electron microscopy (Figure 4) confirms the superlattice structure of this PbS–SCF$_3$ thin film. Here, the oleophobic –CF$_3$ shell, in combination with our thin-film based ligand exchange facilitates close packing of QDs by inducing long-range order. To recreate the same PbS superlattice for TEM, the PbS QD thin film was fabricated on silica terminated TEM grids as illustrated in Fig. 1. The 50 × 50 μm silica windows are approximately similar in dimensions as the channel lengths in the bottom-contact transistors used here. Figure 4 shows the real space TEM image on the left and its associated FFT on the right. Alignment of the PbS QDs can be directly seen in Fig. 4a. More TEM images with their FFTs are in the supporting information (Figure S5 and Figure S6). The interparticle distance given by TEM is 5.6 ± 0.5 nm, close to the 5.8 nm given by GISAXS, slightly larger than the original diameter of the PbS QDs given by their electronic absorption maxima of 5.1 nm. Atomic force microscopy (AFM, **Figure 5**) shows the resultant thin films have thicknesses around 25 – 30 nm, corresponding to 4 – 5 layers of PbS QDs. The superlattice formation here is unexpected, especially since the thin film was spin-coated and not allowed to self-assemble slowly. While both showed long range order, in contrast to the spin-coated thin films, AFM of the dip-coated sample showed a lot of cracks in the PbS–SCF$_3$ film (Fig. S7) since the original long OA ligand of QDs are abruptly removed during ligand exchange.

4) Electrical characterization of thin film

To investigate the effect of long-range order on the transport properties of this PbS–SCF$_3$ thin film, current-voltage transistor measurements were performed in a nitrogen atmosphere. Previous work on PbX (X=S, Se) QDs report that no charge transport in thin film is observed when nanoparticles are functionalized with their original insulating, long-chain ligands; on the other extreme, PbX (X=S, Se) QDs functionalized with EDT or short-chain linear amines (e.g. butylamine) produce thin films where the particles are fused together[34, 41,42-44] and mobilities similar or slightly lower than those reported here. As a control, we fabricated PbS−EDT thin films using the spin-coating procedure illustrated in Fig. 1. Hole mobilities from $1.0 – 4.3 \times 10^{-3}$ cm^2/Vs were obtained, similar to previously reported PbS QD thin films (see Figure S8)[37, 45]. TFT mobilities for the PbS–SCF$_3$ thin films were extracted from transfer curves as described in the Section IIe of the Supporting Information and summarized in **Table 1** and Fig. S9. The source drain current, I$_{DS}$, in these transfer curves are plotted linearly (Figure 5, a – c) and logarithmically (Fig. S10) for clarity. The bottom contact devices were treated with the thiol-based 3-MPTMS SAM and 1H,1H,2H,2H-perfluorodecyltriethoxysilane (see experimental section for details). The transfer and output curves are similar with different surface treatments, suggesting similar structural order in thin film. Since the PbS QDs have a fluorinated shell, we hypothesized that they would preferentially wet a perfluoro-capped surface. Interestingly, under the same spin-coating conditions, a slightly thicker PbS–SCF$_3$ thin film was deposited on the perfluoro SAM (~50 nm compared to 40 nm) with hole mobilities as high as 0.085 cm^2/ Vs. This is close to the hole mobility of PbS QD film reported by Bisri et al with an ion gel to increase carrier density.[45]

In our hands, all PbS–SCF$_3$ thin films give only *p*-type transistors with hole mobilities averaging between 0.002–0.040 cm^2/Vs with on/ off ratios, I$_{ON}$ / I$_{OFF}$ ~10^2. This compares well against state of the art PbS QD TFTs[46-48]. Hole doping of this PbS–SCF$_3$ thin film may be due to cation vacancies or hole transfer to the ligand shell. Cation vacancies may arise from the imbalance in the Pb to S ratio since an extra sulfide anion is supplied with each $\ominus$SCF$_3$ ligand. Figure 6a and 6b show representative output curves from the spin-coated PbS–SCF$_3$ thin film annealed at 60ºC on 3-MPTMS that correspond to the transfer curve in Fig. 5b and AFM in Fig. 5e. The output curves for unannealed spin-coated and dipcoated PbS–SCF$_3$ thin films that correspond to Fig. 5a/d

and Fig. 5c/f are in Fig. S11. This 60℃ annealing step results in an increased ideality in the transfer curves. As can be seen, the square root of the source-drain current, $\sqrt{I_{DS}}$, (black dotted line) has only one slope in Fig 5b, compared to the rest of the transfer curves in Fig. 5a and 5c where at least two slopes are observed. Annealing results in a larger proportion of crystallites oriented out-of-plane as indicated by GISAXS discussed previously. In addition, comparing Fig. 5d, e and f, AFM shows that annealing decreases the RMS roughness of the thin film from 8.9 nm to 5.4 nm.

The mobility of the dipcoated PbS–SCF$_3$ thin film was also investigated. As shown in Fig. S12 and summarized in Table S1, the dipcoated PbS–SCF$_3$ TFTs have hole mobilities as high as 0.025 cm^2/Vs, average mobilities ranging from 0.002–0.007 cm^2/ Vs, and on and off ratios, $I_{ON}/I_{OFF} \sim 10^2$. The lower maximum mobility correlates with the macroscopic cracks and decreased crystallinity of the spin-coated film compared to the dip-coated sample. The hole mobilities of both the dipcoated and spin-coated PbS–SCF$_3$ thin films confirm that $\ominus$SCF$_3$, like other widely investigated short ligands, EDT[37] or formic acid,[49] improve PbS QD thin film transport. Electronic coupling between the QDs is enhanced after replacing the insulating OA ligands on the QD surface as the interparticle distances are decreased to less than 1 nm.
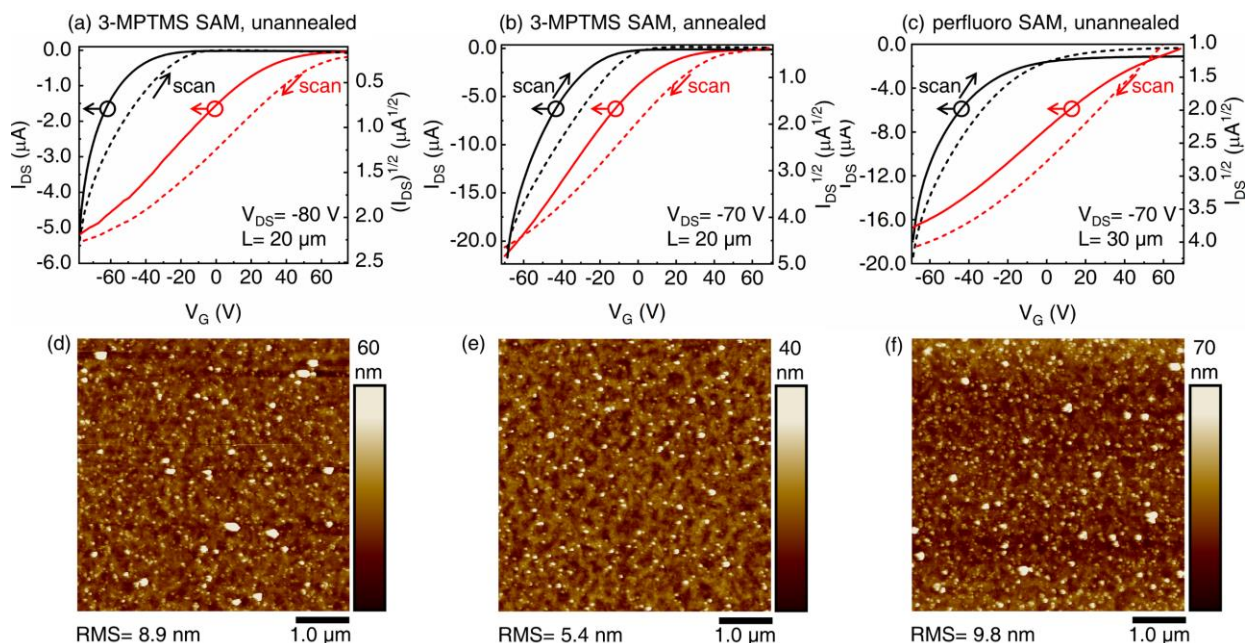

Figure 5. (a–c) Representative transfer curves from spin-coated PbS–SCF$_3$ QD superlattice thin films. The red and black traces represent sweeping towards negative and positive gate voltages (V_G) respectively. (d–f) Corresponding atomic force microscope (AFM) images. (a, b, d and e) represent TFTs with dielectric modified with 3-MPTMS, while (c and f) have the dielectric modified with a perfluoro SAM. Samples (b) and (e) have been annealed at 60℃.

Table 1. Summary of transistor performance, including the maximum and average mobilities, μ_{MAX} and μ_{AVE}, the threshold voltage, V_T, and the on/ off ratios, I_{ON} / I_{OFF} corresponding to PbS QD TFTs in Figure 5. *GISAXS data

| Fabrication methods		Dipcoat		Spin-coated Superlattice					
NCs before film deposition		PbS−OA		PbS−OA+SCF$_3$; OA: SCF$_3$=2:1					
Substrate pretreatment		3-MPTMS thiol SAM						perfluoro SAM	
Film posttreatment		unannealed		unannealed		annealed		unannealed	
Thin film Transistor (TFT)	Scan towards	+V$_G$	−V$_G$	+V$_G$	−V$_G$	+V$_G$	−V$_G$	+V$_G$	−V$_G$
	μ_{MAX} (cm^2/Vs)	0.020	0.005	0.042	0.002	0.079	0.012	0.085	0.012
	μ_{AVE} (cm^2/Vs)	0.006	0.003	0.080	0.002	0.035	0.010	0.018	0.004
	V_T (V)	-10	+30	-10	+60	-10	+50	+10	+70
	I_{ON} / I_{OFF}	200	100	400	100	200	200	20	40
Orientation parallel to substrate*		(111)		(101)				N/A	
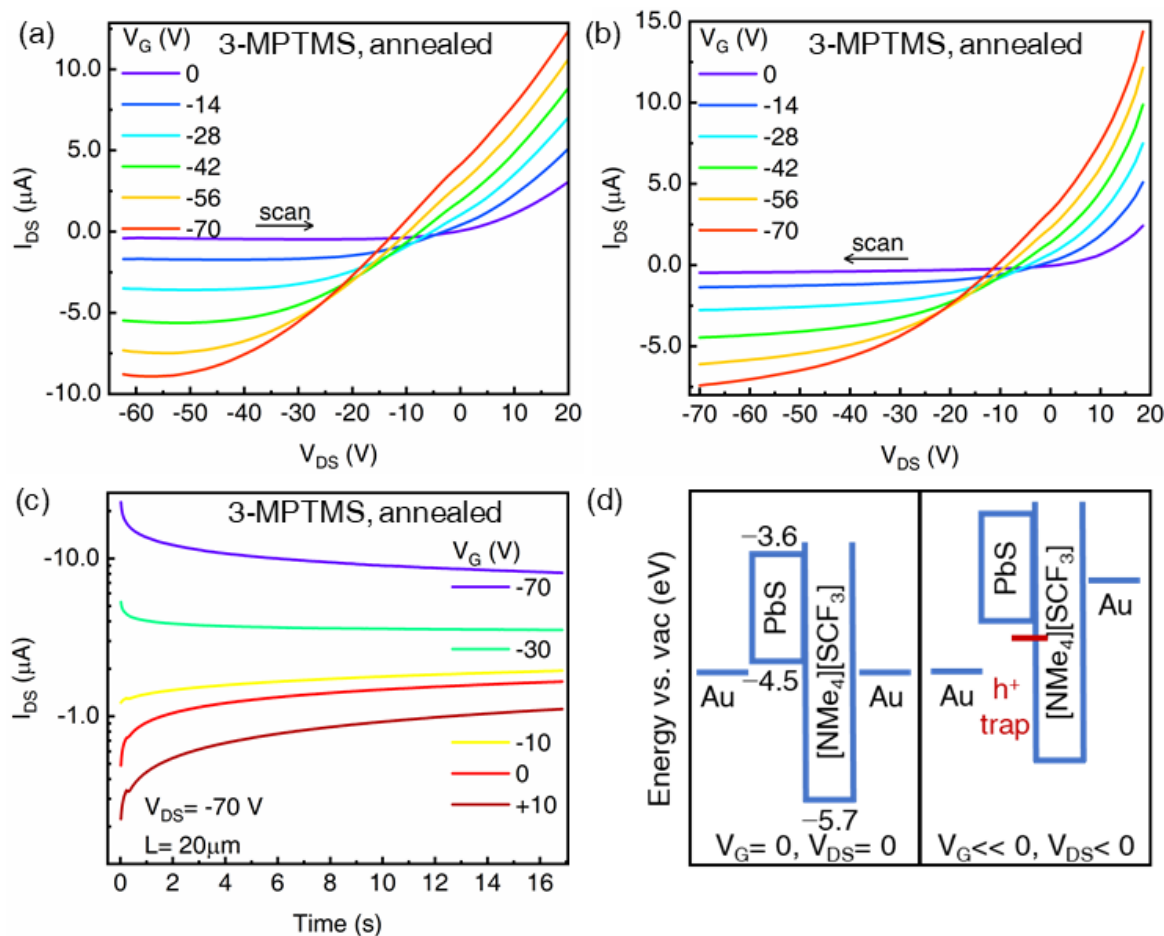
Figure 6. (a) and (b) Typical output curves of annealed PbS–SCF$_3$ QD TFT with 3-MPTMS treatment on the thermal oxide dielectric. (c) Bias stress curves for the same PbS–SCF$_3$ thin films where $V_{DS} = -70$ V is held as the gate voltage, V_G is varied. L = 20 µm. (d) Energy diagram of the PbS−SCF$_3$ QD thin film compared to the highest occupied molecular orbital (HOMO) of [NMe$_4$][SCF$_3$]. The valence band (VB) was obtained by ultraviolet photoelectron spectroscopy (UPS) while the HOMO of [NMe$_4$][SCF$_3$] was obtained in acetonitrile by cyclic voltammetry.

Bias stress curves are consistent with hole traps in this thin film. Bias stress measurements in Figure S13 and Figure 6c show that when $V_{DS} = -70V$, the source-drain current, I_{DS}, decreases over time with negative gate voltage, V_G; the opposite is observed with the application of positive V_G where I_{DS} increases with time. The fact that the dielectric treatment does not affect the general shape of the transfer, output or bias stress curves supports our hypothesis that the charge traps are intrinsic to the PbS–SCF$_3$ QDs and not due to species on the surface of the thermal oxide dielectric (e.g. it has been shown that hydroxyl groups can serve as electron traps.[50]). We note there is no significant change in the hole mobility of this superlattice TFT in a nitrogen glovebox for 7 months.

The hysteresis in these TFT curves may be due to hole traps in the thin film compounded by the common bottom gate that results in a non-negligible gate leakage current (Fig. S14). Fig. 6d shows the conduction and valence bands of the PbS–SCF$_3$ superlattice thin film measured by UPS in comparison with the HOMO of the [NMe$_4$][SCF$_3$] precursor given by cyclic voltammetry. The UPS data was used to determine the valence band energy by fitting the leading edge of the spectra with a parabola and taking the intersection of this parabola with the background as the valence band energy. This procedure was used owing to the low density of states (DOS) at the band edge, which can lead to inaccurate valence band energies when the data is fit on a linear scale.[51] The energy of the conduction band (CB), E_C is approximated by adding the electronic transport gap, E_G of the material to the valence band maximum. E_G is calculated based on the optical absorption and Coulombic stabilization energy (Figure S15 and Table S2).[39] $\ominus$SCF$_3$ HOMO-LUMO levels were obtained by cyclic voltammetry (Fig. S16). The alignment of these energy levels suggests that it is thermodynamically feasible to transfer holes from $\ominus$SCF$_3$ to the QD. The *p*-type doping experimentally observed here may be due to hole transfer from the highest occupied molecular orbital (HOMO) of the thiolate ligand to the valence band (VB) of the PbS QD.

To conclude, we show for the first time fully fluorinated PbS QD superlattice thin films with high hole mobility. The PbS–SCF$_3$ TFTs form *p*-type transistors with mobility as high as 0.085 cm^2/ Vs and on/ off ratios, I_{ON} / I_{OFF} ~10^2. Long-range order is confirmed with GISAXS and TEM measurements. Superlattice formation suggests that this short-fluorinated shell facilitates close-packing of the PbS QDs and induces long-range order. Unfortunately, the thiolate ligands introduce cation vacancies or excess holes in the PbS QD thin film, resulting in unipolar p-type behavior, negating the electron withdrawing nature of the organic CF$_3$ shell. Alternative methods to fluorinate QDs without inadvertent hole doping are being investigated to create the physical conditions for necessary for controlling the band offsets of semiconductor QDs.

Author Contributions
P.X. and M.Q. fabricated the thin film and made current-voltage transistor measurements. P.X. performed synthesis as well as characterized the thin film optically, by AFM and TEM. B.B.P made the GISAXS measurements while D.W.D analyzed the GISAXS data. Z.L. carried out the UPS measurements and data analysis. K.G., Y.D. and M.L.T. oversaw the project. P.X., D.W.D., K.G., Y.D. and M.L.T. wrote the manuscript.

Conflicts of interest
There are no conflicts to declare.

Acknowledgements

Supporting Information

Supporting Information is available online or from the author.

References

1. C. Giansante, R. Mastria, G. Lerario, L. Moretti, I. Kriegel, F. Scotognella, G. Lanzani, S. Carallo, M. Esposito, M. Biasiucci, A. Rizzo and G. Gigli, *Adv. Funct. Mater.*, 2015, **25**, 111-119.

2. A. André, D. Zherebetskyy, D. Hanifi, B. He, M. Samadi Khoshkhoo, M. Jankowski, T. Chassé, L.-W. Wang, F. Schreiber, A. Salleo, Y. Liu and M. Scheele, *Chem. Mater.*, 2015, **27**, 8105-8115.

3. C. Giansante, L. Carbone, C. Giannini, D. Altamura, Z. Ameer, G. Maruccio, A. Loiudice, M. R. Belviso, P. D. Cozzoli, A. Rizzo and G. Gigli, *J. Phys. Chem. C*, 2013, **117**, 13305-13317.

4. A. Andre, M. Weber, K. M. Wurst, S. Maiti, F. Schreiber and M. Scheele, *ACS Appl Mater Interfaces*, 2018, **10**, 24708-24714.

5. A. Andre, D. Zherebetskyy, D. Hanifi, B. He, M. S. Khoshkhoo, M. Jankowski, T. Chasse, L. W. Wang, F. Schreiber, A. Salleo, Y. Liu and M. Scheele, *Chem. Mat.*, 2015, **27**, 8105-8115.

6. D. M. Balazs, D. N. Dirin, H. H. Fang, L. Protesescu, G. H. ten Brink, B. J. Kooi, M. V. Koyalenko and M. A. Loi, *ACS Nano*, 2015, **9**, 11951-11959.

7. D. B. Straus, E. D. Goodwin, E. A. Gaulding, S. Muramoto, C. B. Murray and C. R. Kagan, *J. Phys. Chem. Lett.*, 2015, **6**, 4605-4609.

8. J. H. Choi, A. T. Fafarman, S. J. Oh, D. K. Ko, D. K. Kim, B. T. Diroll, S. Muramoto, J. G. Gillen, C. B. Murray and C. R. Kagan, *Nano Lett.*, 2012, **12**, 2631-2638.

9. R. W. Crisp, D. M. Kroupa, A. R. Marshall, E. M. Miller, J. Zhang, M. C. Beard and J. M. Luther, *Sci Rep*, 2015, **5**, 9945.

10. X. Z. Lan, O. Voznyy, F. P. G. de Arquer, M. X. Liu, J. X. Xu, A. H. Proppe, G. Walters, F. J. Fan, H. R. Tan, M. Liu, Z. Y. Yang, S. Hoogland and E. H. Sargent, *Nano Lett.*, 2016, **16**, 4630-4634.

11. F. Mongin, L. Mojovic, B. Guillamet, F. Trecourt and G. Queguiner, *J. Org. Chem.*, 2002, **67**, 8991-8994.

12. H. Zhang, J. Jang, W. Liu and D. V. Talapin, *ACS Nano*, 2014, **8**, 7359-7369.

13.   J. Tang, K. W. Kemp, S. Hoogland, K. S. Jeong, H. Liu, L. Levina, M. Furukawa, X. H. Wang, R. Debnath, D. K. Cha, K. W. Chou, A. Fischer, A. Amassian, J. B. Asbury and E. H. Sargent, *Nat Mater*, 2011, **10**, 765-771.

14.   A. H. Ip, S. M. Thon, S. Hoogland, O. Voznyy, D. Zhitomirsky, R. Debnath, L. Levina, L. R. Rollny, G. H. Carey, A. Fischer, K. W. Kemp, I. J. Kramer, Z. Ning, A. J. Labelle, K. W. Chou, A. Amassian and E. H. Sargent, *Nat Nanotechnol*, 2012, **7**, 577-582.

15.   G. H. Kim, F. P. G. de Arquer, Y. J. Yoon, X. Z. Lan, M. X. Liu, O. Voznyy, Z. Y. Yang, F. J. Fan, A. H. Ip, P. Kanjanaboos, S. Hoogland, J. Y. Kim and E. H. Sargent, *Nano Lett.*, 2015, **15**, 7691-7696.

16.   A. T. Fafarman, W. K. Koh, B. T. Diroll, D. K. Kim, D. K. Ko, S. J. Oh, X. Ye, V. Doan-Nguyen, M. R. Crump, D. C. Reifsnyder, C. B. Murray and C. R. Kagan, *J. Am. Chem. Soc.*, 2011, **133**, 15753-15761.

17.   M. V. Kovalenko, M. Scheele and D. V. Talapin, *Science*, 2009, **324**, 1417-1420.

18.   A. Nag, M. V. Kovalenko, J. S. Lee, W. Y. Liu, B. Spokoyny and D. V. Talapin, *J. Am. Chem. Soc.*, 2011, **133**, 10612-10620.

19.   A. T. Fafarman, S. H. Hong, H. Caglayan, X. Ye, B. T. Diroll, T. Paik, N. Engheta, C. B. Murray and C. R. Kagan, *Nano Lett.*, 2013, **13**, 350-357.

20.   Z. Ning, H. Dong, Q. Zhang, O. Voznyy and E. H. Sargent, *ACS Nano*, 2014, **8**, 10321-10327.

21.   A. H. Ip, A. Kiani, I. J. Kramer, O. Voznyy, H. F. Movahed, L. Levina, M. M. Adachi, S. Hoogland and E. H. Sargent, *ACS Nano*, 2015, **9**, 8833-8842.

22.   C. R. Kagan, E. Lifshitz, E. H. Sargent and D. V. Talapin, *Science*, 2016, **353**.

23.   Y. Liu, M. Gibbs, J. Puthussery, S. Gaik, R. Ihly, H. W. Hillhouse and M. Law, *Nano Lett.*, 2010, **10**, 1960-1969.

24.   H. Zhang, J. M. Kurley, J. C. Russell, J. Jang and D. V. Talapin, *J. Am. Chem. Soc.*, 2016, **138**, 7464-7467.

25.   J. Xu, O. Voznyy, M. Liu, A. R. Kirmani, G. Walters, R. Munir, M. Abdelsamie, A. H. Proppe, A. Sarkar, F. P. Garcia de Arquer, M. Wei, B. Sun, M. Liu, O. Ouellette, R. Quintero-Bermudez, J. Li, J. Fan, L. Quan, P. Todorovic, H. Tan, S. Hoogland, S. O. Kelley, M. Stefik, A. Amassian and E. H. Sargent, *Nat Nanotechnol*, 2018, **13**, 456-462.

26.   J. H. Choi, A. T. Fafarman, S. J. Oh, D. K. Ko, D. K. Kim, B. T. Diroll, S. Muramoto, J. G. Gillen, C. B. Murray and C. R. Kagan, *Nano Lett.*, 2012, **12**, 2631-2638.

27.   J. S. Lee, M. V. Kovalenko, J. Huang, D. S. Chung and D. V. Talapin, *Nat. Nanotechnol.*, 2011, **6**, 348-352.

28.   E. Talgorn, Y. N. Gao, M. Aerts, L. T. Kunneman, J. M. Schins, T. J. Savenije, M. A. van Huis, H. S. J. van der Zant, A. J. Houtepen and L. D. A. Siebbeles, *Nat. Nanotechnol.*, 2011, **6**, 733-739.

29.   I.-H. Chu, M. Radulaski, N. Vukmirovic, H.-P. Cheng and L.-W. Wang, *J. Phys. Chem. C*, 2011, **115**, 21409-21415.

30.   C. Qian, W. Sun, L. Wang, C. Chen, K. Liao, W. Wang, J. Jia, B. D. Hatton, G. Casillas, M. Kurylowicz, C. M. Yip, M. L. Mastronardi and G. A. Ozin, *J. Am. Chem. Soc.*, 2014, **136**, 15849-15852.

31.   C. H. Chuang, P. R. Brown, V. Bulovic and M. G. Bawendi, *Nat Mater*, 2014, **13**, 796-801.

32.   P. Xia, Z. Liang, M. Mahboub, J. van Baren, C. H. Lui, J. Jiao, K. R. Graham and M. L. Tang, *Chem. Mater.*, 2018, **30**, 4943-4948.

33.   C. R. Kagan, C. B. Murray, M. Nirmal and M. G. Bawendi, *Phys. Rev. Lett.*, 1996, **76**, 1517-1520.
34.   D. M. Balazs, B. M. Matysiak, J. Momand, A. G. Shulga, M. Ibanez, M. V. Kovalenko, B. J. Kooi and M. A. Loi, *Adv. Mater.*, 2018, **30**, e1802265.
35.   Z. Jiang, *J. Appl. Crystallogr.*, 2015, **48**, 917-926.
36.   D. M. Smilgies, A. T. Heitsch and B. A. Korgel, *J. Phys. Chem. B*, 2012, **116**, 6017-6026.
37.   T. P. Osedach, N. Zhao, T. L. Andrew, P. R. Brown, D. D. Wanger, D. B. Strasfeld, L.-Y. Chang, M. G. Bawendi and V. Bulović, *ACS Nano*, 2012, **6**, 3121-3127.
38.   G. I. Koleilat, L. Levina, H. Shukla, S. H. Myrskog, S. Hinds, A. G. Pattantyus-Abraham and E. H. Sargent, *ACS Nano*, 2008, **2**, 833-840.
39.   P. R. Brown, D. Kim, R. R. Lunt, N. Zhao, M. G. Bawendi, J. C. Grossman and V. Bulovic, *ACS Nano*, 2014, **8**, 5863-5872.
40.   E. A. Gaulding, B. T. Diroll, E. D. Goodwin, Z. J. Vrtis, C. R. Kagan and C. B. Murray, *Adv. Mater.*, 2015, **27**, 2846-+.
41.   M. M. R. Moayed, T. Bielewicz, H. Noei, A. Stierle and C. Klinke, *Adv. Funct. Mater.*, 2018, **28**, 1706815.
42.   K. Whitham, J. Yang, B. H. Savitzky, L. F. Kourkoutis, F. Wise and T. Hanrath, *Nat Mater*, 2016, **15**, 557-563.
43.   S. Maiti, S. Maiti, A. Maier, J. Hagenlocher, A. Chumakov, F. Schreiber and M. Scheele, *J. Phys. Chem. C*, 2019, **123**, 1519-1526.
44.   M. C. Weidman, Q. Nguyen, D. M. Smilgies and W. A. Tisdale, *Chem. Mat.*, 2018, **30**, 807-816.
45.   S. Z. Bisri, C. Piliego, M. Yarema, W. Heiss and M. A. Loi, *Adv. Mater.*, 2013, **25**, 4309-4314.
46.   D. M. Balazs and M. A. Loi, *Adv, Mater.*, 2018, **30**, 1800082.
47.   R. Wang, Y. Shang, P. Kanjanaboos, W. Zhou, Z. Ning and E. H. Sargent, *Energy Environ. Sci.*, 2016, **9**, 1130-1143.
48.   D. Bederak, D. M. Balazs, N. V. Sukharevska, A. G. Shulga, M. Abdu-Aguye, D. N. Dirin, M. V. Kovalenko and M. A. Loi, *ACS Appl. Nano. Mater.*, 2018, **1**, 6882-6889.
49.   M. H. Zarghami, Y. Liu, M. Gibbs, E. Gebremichael, C. Webster and M. Law, *ACS Nano*, 2010, **4**, 2475-2485.
50.   L. L. Chua, J. Zaumseil, J. F. Chang, E. C. Ou, P. K. Ho, H. Sirringhaus and R. H. Friend, *Nature*, 2005, **434**, 194-199.
51.   E. M. Miller, D. M. Kroupa, J. Zhang, P. Schulz, A. R. Marshall, A. Kahn, S. Lany, J. M. Luther, M. C. Beard, C. L. Perkins and J. van de Lagemaat, *ACS Nano*, 2016, **10**, 3302-3311.

Table of Contents

Keyword: superlattice, quantum dots, film transistor, fluorine, lead sulfide

P. Xia, D.W. Davies, B. B. Patel, M. Qin, Z. Liang, K. R. Graham, Y. Diao and M. L. Tang*

Title: Spin-coated fluorinated PbS QD superlattice thin film with high hole mobility
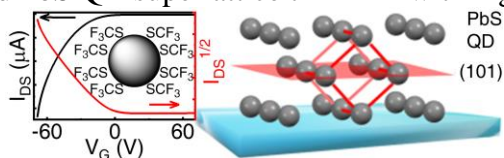
A simple spincoating method was used to fabricate lead sulfide quantum dot superlattice thin films functionalized with a short fully fluorinated trifluoromethylthiolate ligand ($\ominus$SCF$_3$). Transmission electron microscopy and grazing incident small angle X-ray scattering indicates a cubic superlattice. Hole mobilities as high as 0.085 cm^2/Vs were obtained from thin film transistor current-voltage measurements.